Modeling, analysis, and design of stationary reference frame droop controlled parallel three-phase voltage source inverters

Vasquez, Juan Carlos; Guerrero, Josep M.; Savaghebi, Mehdi; Teodorescu, Remus

Published in:
Proceedings of the 8th IEEE International Conference on Power Electronics and ECCE Asia (ICPE & ECCE 2011)

DOI (link to publication from Publisher):
10.1109/ICPE.2011.5944601

Publication date:
2011

Document Version
Early version, also known as pre-print

Modeling, Analysis, and Design of Stationary Reference Frame Droop Controlled Parallel Three-Phase Voltage Source Inverters

Juan C. Vasquez[2], Josep M. Guerrero[1,2], Mehdi Savaghebi[3], and Remus Teodorescu[2]
[1] Departament d'Enginyeria de Sistemes, Automàtica i Informàtica Industrial, Universitat Politècnica de Catalunya
[2] Department of Energy Technology, Institute of Aalborg University
[3] Center of Excellence for Power System Automation and Operation, Iran University of Science and Technology
Email: juq@et.aau.dk , joz@et.aau.dk

***Abstract*- Power electronics based microgrids consist of a number of voltage source inverters (VSIs) operating in parallel. In this paper, the modeling, control design, and stability analysis of parallel connected three-phase VSIs are derived. The proposed voltage and current inner control loops and the mathematical models of the VSIs were based on the stationary reference frame. A hierarchical control for the paralleled VSI system was developed based on three levels. The primary control includes the droop method and the virtual impedance loops, in order to share active and reactive power. The secondary control restores the frequency and amplitude deviations produced by the primary control. And the tertiary control regulates the power flow between the grid and the microgrid. Also, a synchronization algorithm is presented in order to connect the microgrid to the grid. The evaluation of the hierarchical control is presented and discussed. Experimental results are provided to validate the performance and robustness of the VSIs functionality during islanded and grid-connected operations, allowing a seamless transition between these modes through control hierarchies by regulating frequency and voltage, main-grid interactivity, and to manage power flows between the main grid and the VSIs.**

Keywords: **Distributed Generation (DG), Droop method, Hierarchical control, Microgrid (MG), Voltage Source Inverters.**

I. INTRODUCTION

RECENTLY, MicroGrids (MGs) are emerging as a possibility of test future SmartGrid issues in small scale. In addition, power electronics-based MGs are useful when integrating renewable energy resources, distributed energy storage systems and active loads. Indeed, power electronics equipment is used as interface between those devices and the MG. This way, MG can deal with power quality issues as well as increase its interactivity with the main grid or with other MGs, creating MG clusters [1].

Voltage source inverters (VSIs) are often used as a power electronics interface; hence, parallel VSIs control forming a MG has been investigated in the last years [1-9]. Decentralized and cooperative controllers such as the droop method have been proposed in the literature. Further, in order to increase the reliability and performances of the droop controlled VSIs, virtual impedance control algorithms have been also developed, providing to the inverters hot-swap operation, harmonic power sharing and robustness for large line power impedances variations [10].

Droop control is a kind of collaborative control used for share active and reactive power between VSIs in a cooperative way. It can be seen as a primary power control of synchronous machine. However, the price to pay is that the power sharing is obtained through voltage and frequency deviations of the system [11], [12]. Thus, secondary controllers are proposed in order to reduce those deviations, like those in large electric power systems [1]. Hence, the MG can operate in island, restoring the frequency and amplitude deviations created by the total amount of active and reactive power demanded by the load [11].

In the case of transferring from islanded operation to grid connected mode, it is necessary to first synchronize the MG to the grid. Thus, a distributed synchronization control algorithm is necessary [1]. Once the synchronization is reached, a static transfer switch connects the MG to the grid or to a MG cluster. After the transfer process between islanded and grid-connected modes is finished, it is necessary to control the active and reactive power flows at the common coupling point (PCC). This can be done by a tertiary controller that should take into account state of charge (SoC) of the energy storage systems, available energy generation, and energy demand [7,13]. These aspects are out of the scope of this paper.

In this paper a hierarchical control for a parallel VSI system was developed by using stationary reference frame and hierarchical control. The inner control loops of the VSIs where based on current and voltage resonant controllers. Active and reactive power calculations have been used to droop the frequency and amplitude of the individual VSIs voltage references and a virtual impedance loop has been included. A MG central controller that includes a secondary control and a coordinated synchronization control loop have been developed in order to restore frequency and amplitude in the MG and to synchronize it to the grid.

The paper is organized as follows. Section II, the system modeling and the control design of the voltage and current control loops are presented. Section III shows the droop control and virtual impedance loop designs. Section IV proposes a coordinated synchronization control loop for the MG. Section V presents the secondary control of frequency and voltage. The simulation results are shown in Section VI. Section VII presents the experimental results of a paralleled two 2.2kW-inverter system. Finally, Section VIII concludes the paper.

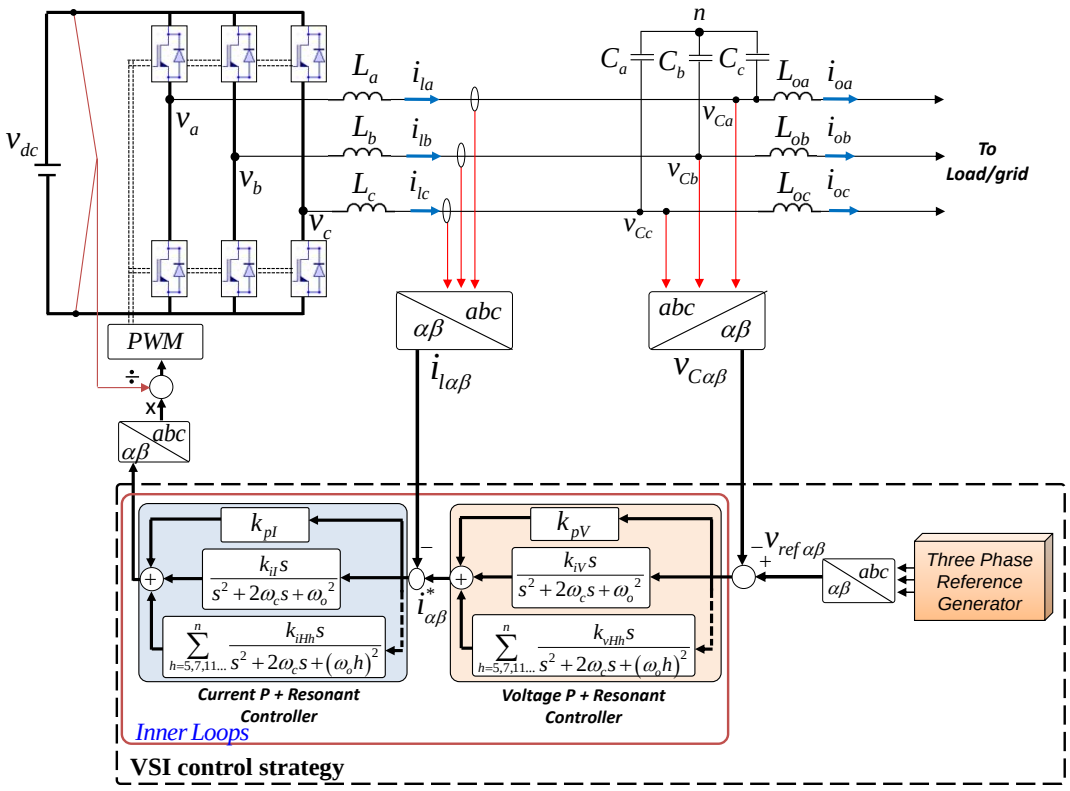

Fig.1. Block diagram of the inner control loops of a three phase VSI.

II. Inner Control Design

The control proposed for the paralleled VSI system is based on the droop control framework, which includes voltage and current control loops, the virtual impedance loop, and the droop control strategy.Fig. 1 shows the power stage of a VSI consisting of a three phase PWM inverter and an LCL filter. The proposed controller is based on the stationary reference frame, including a voltage and a current control loops. These control loops includes proportional + resonant (PR) terms tuned at the fundamental frequency and the harmonics 5th, 7th, and 11th. Notice that both current and voltage loops need harmonic terms to give the harmonic current needed and to suppress the harmonic voltage content, respectively [4].

The voltage and current controllers are based on a PR structure, where generalized integrators (GI) are used to achieve zero steady-state error. For consistency and simplicity, the plant and the controller are modeled in stationary reference frame, avoiding the use of DQ transformations for each harmonic term, which generates pair inter-harmonics hard to deal with.

As a three-phase system can be modeled as two independent single-phase systems based on the *abc*/$\alpha\beta$ coordinate transformation principle, the control diagram can be expressed and simplified as depicted in Fig 2.

In order to analyze the closed-loop dynamics of the system, the Mason's theorem is applied for block diagram reduction purposes and the following transfer function is derived from Fig. 3:

$$V_c = \frac{G_v(s)G_i(s)G_{PWM}}{LCs^2+\left(Cs+G_v(s)\right)G_i(s)G_{PWM}+1}V_{ref} - \frac{\frac{1}{Cs}}{LCs^2+\left(Cs+G_v(s)\right)G_i(s)G_{PWM}+1}i_o \quad (1)$$

being V_{ref} the voltage reference, i_o the output current, L the filter inductor value and C the filter capacitor value. The transfer functions of the voltage controller, current controller and PWM delay, shown in (1), are described as following:

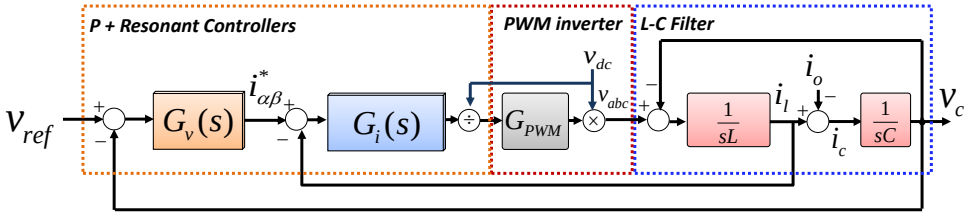

Fig. 2. Block diagram of the closed-loop VSI.

$$G_v(s) = k_{pV} + \frac{k_{rV}s}{s^2+\omega_o^2} + \sum_{h=5,7,11} \frac{k_{hV}s}{s^2+(\omega_o h)^2} \quad (2)$$

$$G_i(s) = k_{pI} + \frac{k_{rI}s}{s^2+\omega_o^2} + \sum_{h=5,7,11} \frac{k_{hI}s}{s^2+(\omega_o h)^2} \quad (3)$$

$$G_{PWM} = \frac{1}{1+1.5T_s} \quad (4)$$

where k_{pV} and k_{pI} are the proportional term coefficients, k_{rV} and k_{rI} are the resonant term coefficients at ω_o = 50 Hz, k_{hV} and k_{hI} are the resonant coefficient terms for the harmonics h (5th, 7th, and 11th), and T_s is the sampling time.

By using the closed loop model described by equations (1)-(4), the influence of the control parameters over the fundamental frequency can be analyzed by using the Bode diagrams shown in Fig. 3. Notice that the control objective is to achieve a band pass filter closed loop behavior with narrow bandwidth, with 0dB of gain, but also avoiding resonances in the boundary.

Fig. 4 shows similar bode families regarding 5th and 7th harmonic tracking. Harmonic current tracking is required for both current and voltage loops. Not only current control loop includes current harmonic tracking in order to supply nonlinear currents to nonlinear loads, but also voltage control loop includes that since it is necessary to suppress voltage harmonics produced by this kind of loads.

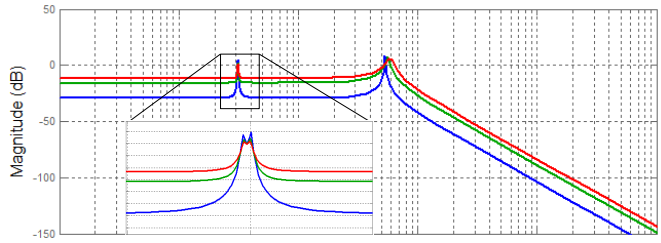

Fig.3. Bode plot of the sensitivity transfer function for different parameters of the PR controllers without harmonic compensation. a) k_{pV} = [0.1 1] and k_{pI} = 1 and b) k_{pV} = 0.3 and k_{pI} = [0.1 1].

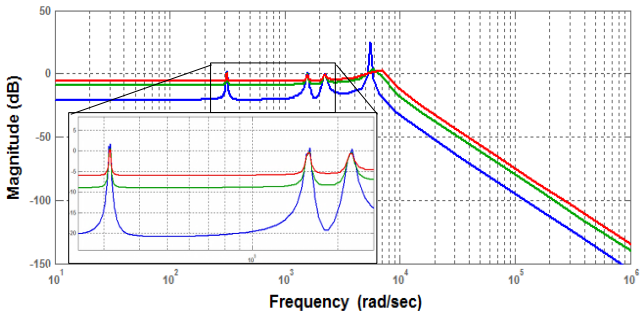

Fig.4. Bode plot of sensitivity transfer function for different PR controllers with 5th and 7th harmonic compensation. k_{pV} = [0.1 1] and k_{pI} = 1.

III. Droop Control and Virtual Impedance Loop

With the objective to parallel connect the VSI units, the reference v_{ref} of the voltage control loop will be generated by means of an individual luck-up table, together with the droop controller and a virtual impedance loop. The droop control is responsible to adjust the phase and the amplitude of the voltage reference according to the active and reactive powers (P and Q), hence ensuring P and Q flow control.

The droop control functions can be defined as following:

$$\phi = \phi^* - G_p(s)\left(P - P^*\right) \quad (5)$$

$$E = E^* - G_Q(s)\left(Q - Q^*\right) \quad (6)$$

being ϕ the phase of V_{ref}, ϕ^* is the phase reference $\phi^* = \omega^* \int dt = \omega^* t$, P^* and Q^* are the active and reactive references normally settled to zero, and $G_p(s)$ and $G_Q(s)$ are the compensator function, which are selected as following:

$$G_P(s) = \frac{k_{pP}s + k_{iP}}{s} \quad (7)$$

$$G_Q(s) = k_{pQ} \quad (8)$$

being k_{iP} and k_{pQ} the static droop coefficients, while k_{pP} can be considered as a virtual inertia of the system, also known as transient droop term. The static droop coefficients k_{iP} and k_{pQ} can be selected taking into account the following relationships $k_{iP} = \Delta f/\Delta P$ (maximum frequency deviation/nominal active power) and $k_{pQ} = \Delta V/\Delta Q$ (maximum amplitude deviation/nominal reactive power).

Fig. 6 shows the block diagram of the droop control implementation. It consists of a power block calculation that calculates P and Q in the $\alpha\beta$-coordinates by using the following well-known relationship [16]:

$$p = v_{c\alpha} \cdot i_{o\alpha} + v_{c\beta} \cdot i_{o\beta} \quad (9)$$

$$q = v_{c\beta} \cdot i_{o\alpha} - v_{c\alpha} \cdot i_{o\beta} \quad (10)$$

being p and q active and reactive power before filtering, $v_{c\alpha\beta}$ and $i_{c\alpha\beta}$ the capacitor voltage and the filter current. In order to eliminate p and q ripples, the following low pass filters are applied to obtain P and Q:

$$P = \frac{\omega_c}{s+\omega_c} p \quad (11)$$

$$Q = \frac{\omega_c}{s+\omega_c} q \quad (12)$$

being ω_c the cut-off frequency of the low-pass filters.

Finally the voltage reference can be obtained by using the following equation:

$$v_{ref} = E\sin(\phi) \quad (13)$$

being E the amplitude determined by (6) and ω the frequency determined by (5) and $\phi = \omega \int dt = \omega t$.

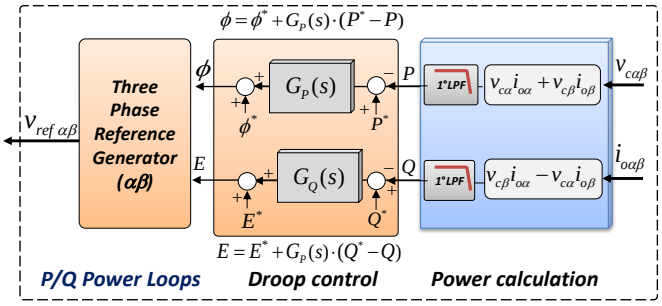

Fig.6. Block diagram of the droop controller.

The reference v_{ref} frequency and amplitudes are controlled by the droop functions, generated in *abc* and transformed to $\alpha\beta$-coordinates. The $\alpha\beta$-coordinates variables are obtained by using the well-know transformation:

$$\begin{bmatrix} v_\alpha \\ v_\beta \end{bmatrix} = \sqrt{2/3}\cdot\begin{bmatrix} 1 & -1/2 & -1/2 \\ 0 & \sqrt{3}/2 & -\sqrt{3}/2 \end{bmatrix}\cdot\begin{bmatrix} v_a \\ v_b \\ v_c \end{bmatrix} \tag{14}$$

This transformation have been used for currents and voltages from *abc* to $\alpha\beta$. This way our system can be regarded as two single phase systems.

In addition, a virtual impedance loop has been added to the voltage reference in order to fix the output impedance of the VSI which will determine the P/Q power angle/amplitude relationships that will determine the droop method control law.

Fig 7 depicts the implementation of the virtual impedance loop. Although the series impedance of a generator is mainly inductive due to the LCL filter, the virtual impedance can be chosen arbitrarily. In contrast with physical impedance, this virtual output impedance has no power losses, and it is possible to implement resistance without efficiency losses. The virtual impedance loop can be expressed as following in $\alpha\beta$-coordinates [14]:

$$\begin{cases} v_{v\alpha} = R_v \cdot i_{o\alpha} - \omega L_v \cdot i_{o\beta} \\ v_{v\beta} = R_v \cdot i_{o\beta} + \omega L_v \cdot i_{o\alpha} \end{cases} \tag{15}$$

being R_V and L_V the virtual resistance and inductance value, and $v_{v\alpha,\beta}$ and $i_{o\alpha,\beta}$ the voltage and output current in $\alpha\beta$-frame. Taking into account the virtual voltage drop across the virtual impedance $v_{v\alpha,\beta}$ is subtracted from the voltage reference, we can calculate the output impedance of the closed-loop system:

$$Z_o(s) = \frac{1/Cs + G_v(s)G_i(s)G_{PWM}(s)Z_D(s)}{LCs^2 + (Cs + G_v(s))G_i(s)G_{PWM}(s) + 1} + L_o s \tag{16}$$

being L_o the output inductor of the *LCL* filter.

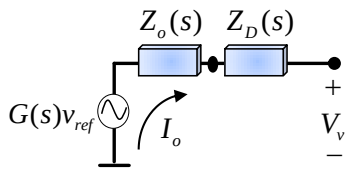

Fig.7. Thévenin equivalent circuit of the closed-loop VSI.

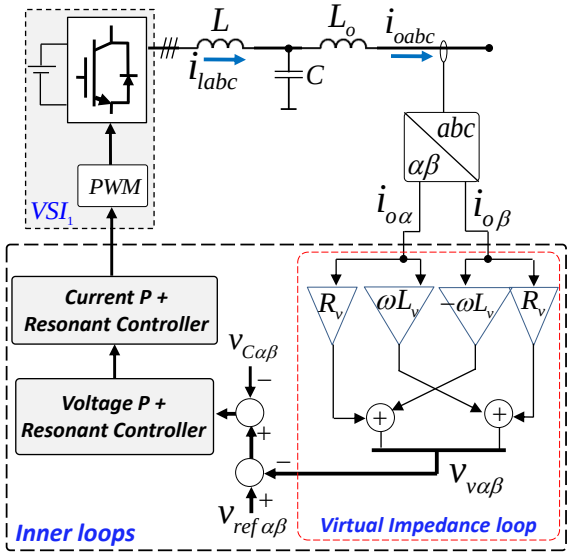

Fig.8. Implementation of the virtual output impedance in $\alpha\beta$-coordinates.

The closed-loop model of the VSI can be represented by means of the Thévenin equivalent circuit shown in Fig. 8, which can be expressed as:

$$v_{out}(s) = G(s)v_{ref} - Z_o(s)i_o \tag{17}$$

being v_{out} the output voltage of the VSI considering the LCL filter, the voltage and current control loops and the virtual impedance loop.

By analyzing the closed loop output impedance $Z_o(s)$, we can obtain the Bode plot shown in Fig. 9. Note that for 50 Hz a phase of 90º is obtained hence being mainly inductive.

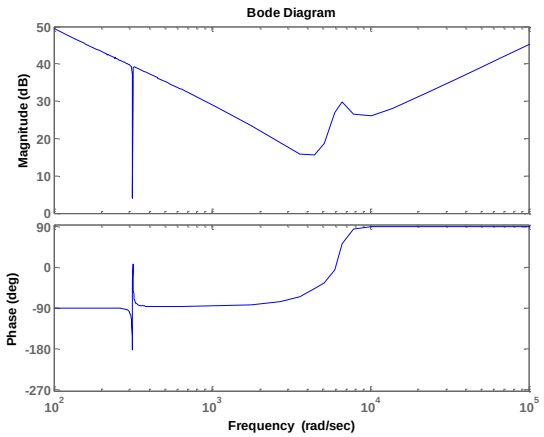

Fig.9. Bode plot of the output impedance.

IV. Coordinated Synchronization Loop

The droop control can be used in both islanded and grid connected modes. In order to synchronize all the VSI of the MG, a coordinated synchronization loop is necessary to synchronize the MG with the grid. In this section, a

synchronization control loop in stationary reference frame is proposed as shown in Fig. 10.

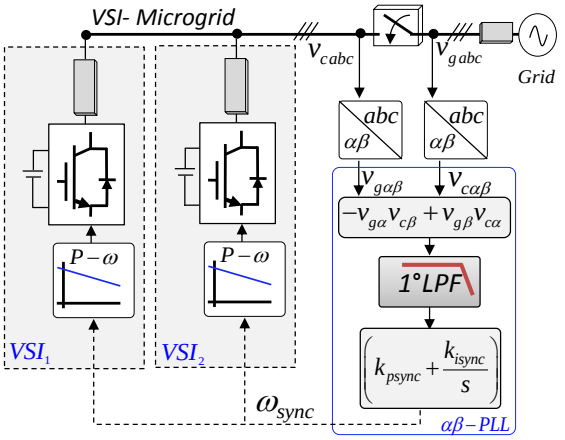

Fig.10. Block diagram the synchronization control loop of a droop controlled MG

The synchronization process is done by using the variables $v_{g\alpha\beta}$ and $v_{c\alpha\beta}$ as the alpha-beta components of the grid and the VSI voltages. Thus, when both voltages are synchronized, we can assume that

$$\left\langle v_{g\beta}v_{c\alpha}-v_{g\alpha}v_{c\beta}\right\rangle=0 \tag{18}$$

being <*x*> the average value of the variable *x* over the line frequency. Thus, we can easily derive the following PLL structure, which consist of this orthogonal product, a low-pass filter and a PI controller:

$$\omega_{sync}=\left(v_{g\beta}v_{c\alpha}-v_{g\alpha}v_{c\beta}\right)\frac{\omega_c}{s+\omega_c}\frac{k_p s+k_i}{s} \tag{18}$$

where k_p and k_i are the coefficients of the PI, and the signal ω_{sync} is the output of the coordinated-PLL to be sent to each VSI to adjust their individual *P*-ω droop function. Notice that by using frequency data is suitable for low bandwidth communications, instead of using phase or time domain information, which would need critical high-speed communications. This algorithm also reduces computational requirement without hampering the P/Q control loop performances.

The signal ω_{sync} is added by each individual VSI, integrating and adding over the phase of the system, as can be seen in Fig. 6.

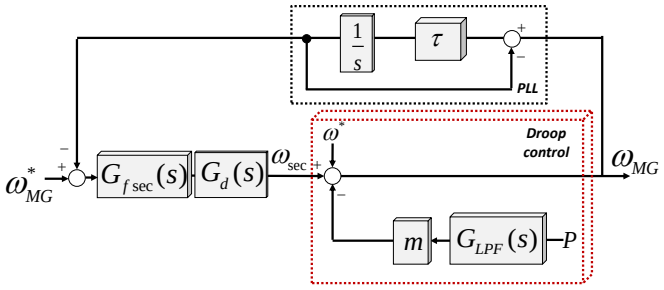

Fig.11. Block diagram the frequency secondary control.

V. SECONDARY CONTROL FOR VOLTAGE-FREQUENCY RESTORATION

The secondary control is responsible of removing any steady-state error introduced by the droop control [15,16]. The frequency and amplitude restoration compensators can be derived as [13]:

$$\omega_{rest}=k_{pF}\left(\omega^*_{MG}-\omega_{MG}\right)+k_{iF}\int\left(\omega^*_{MG}-\omega_{MG}\right)dt \tag{19}$$

$$E_{rest}=k_{pE}\left(E^*_{MG}-E_{MG}\right)+k_{iE}\int\left(E^*_{MG}-E_{MG}\right)dt \tag{20}$$

being $k_{p\omega}$, $k_{i\omega}$, k_{pE}, and k_{iE} the control parameters of the secondary control compensator. In this case, ω_{rest} and E_{rest} must be limited in order to do not exceed the maximum allowed frequency and amplitude deviations. Fig. 12 shows the overall control system, considering current and voltage control loops, virtual output impedances, droop controllers, and secondary control of a MG.

A. FREQUENCY RESTORATION SECONDARY CONTROL

In order to analyze the system stability and to adjust the parameters of the frequency secondary control, a model has been developed, as can be seen in Fig. 11. The control block diagram includes the droop control of the system (m=k_{iP}), the simplified PLL first-order transfer function used to extract the frequency of the MG, and the secondary control $G_{fsec}(s)$, followed by a delay $G_d(s)$ produced by the communication lines.

From the block diagram we can obtain the following model:

$$\omega_{MG}=\frac{G_{f\,sec}(s)G_d(s)}{1+G_{f\,sec}(s)G_d(s)G_{PLL}(s)}\omega^*_{MG}-\frac{mG_{LPF}(s)}{1+G_{f\,sec}(s)G_d(s)G_{PLL}(s)}P \tag{15}$$

where the transfer functions can be expressed as follows:

$$G_{f\,sec}(s)=\frac{k_{pF}s+k_{iF}}{s}, \tag{16}$$

$$G_{PLL}(s)=\frac{1}{s/\tau+1}, \tag{17}$$

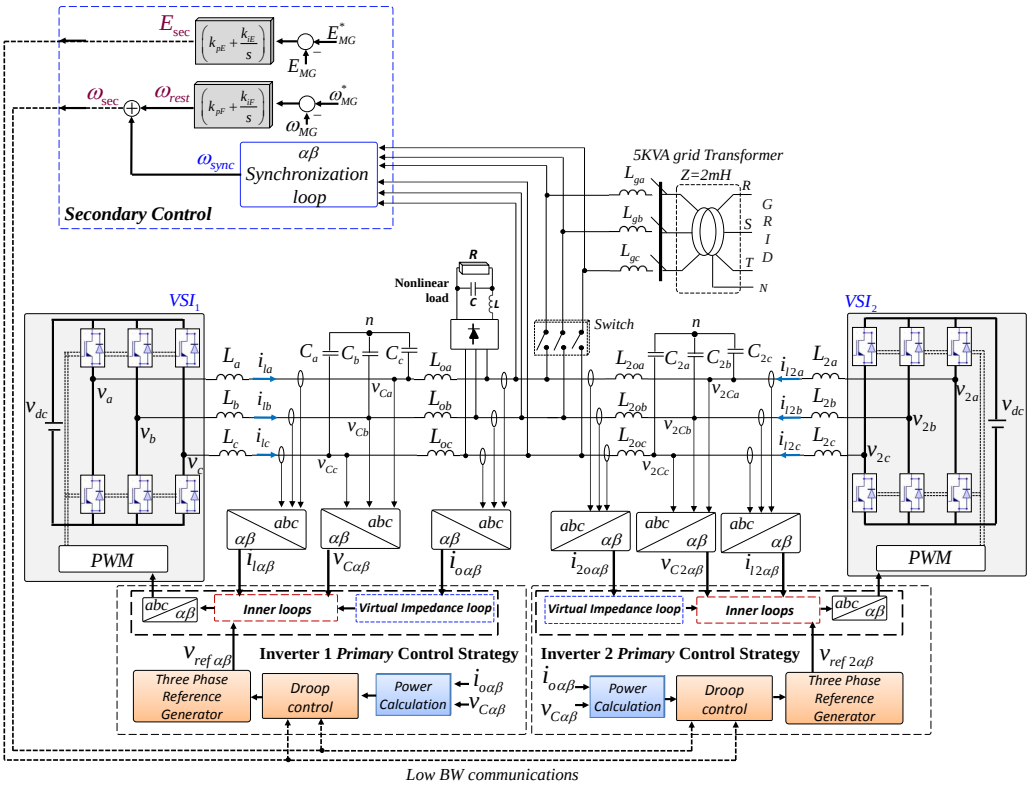

Fig. 12. Block diagram of the whole control system of two VSIs forming a MG.

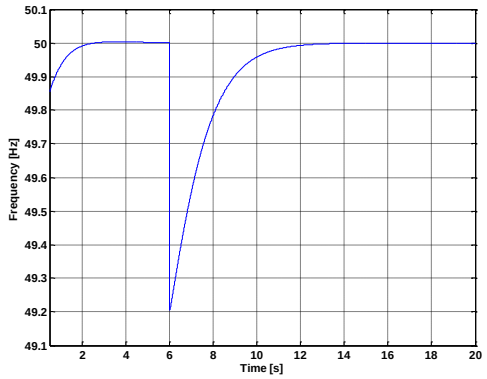

Fig. 13. Transient response of the frequency secondary control model.

$$G_d(s) = \frac{1}{s+1.5}, \tag{18}$$

$$G_{LPF}(s) = \frac{\omega_c}{s+\omega_c}, \tag{19}$$

Thus, the closed loop transfer function P-to-ω_{MG} can be expressed as following:

$$\omega_{MG} = -\frac{m\omega_c s\left(s^2 + sa + b\right)}{s^4 + s^3 c + s^2 d + se + f} P \tag{20}$$

with the following parameters:

$$a = \tau + 1.5$$
$$b = 1.5\tau$$
$$c = 1.5 + \omega_c + \tau$$
$$d = \omega_c(1.5+\tau) + \tau(1.5 + k_{pF})$$
$$e = \tau(\omega_c(k_{pF} + 1.5) + k_{iF})$$
$$f = \tau k_{iF}\omega_c$$

Fig. 13 depicts the step response of the model (20) for a P step change. This model allows us to adjust properly the control parameters of the secondary control and to study the limitations of the communications delay.

B. *Amplitude restoration secondary control*

Similar procedure has been applied when designing the voltage secondary controller. Fig. 14 shows the block diagram obtained in this case.

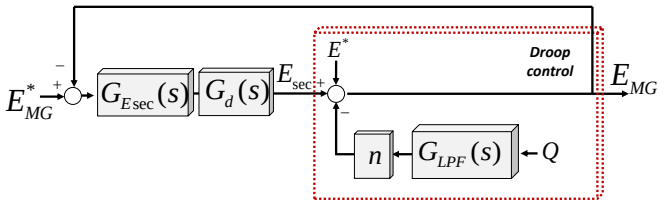

Fig.14. Block diagram of the amplitude secondary control.

Similarly, we can obtain the closed loop voltage dynamic model:

$$E_{MG}^{*} = \frac{G_{E\sec}(s)G_d(s)}{1+G_{E\sec}(s)G_d(s)}E_{\sec} - \frac{nG_{LPF}(s)}{1+G_{E\sec}(s)G_d(s)}Q \quad (15)$$

where the transfer function G_{Esec} is defined as following

$$G_{E\sec}(s) = \frac{k_{pE}s + k_{iE}}{s}, \quad (16)$$

Consequently, the following transfer function Q-to-E_{MG} can be obtained:

$$E_{MG} = -\frac{n\omega_c s(s+1.5)}{s^3 + as^2 + bs + k_{iE}\omega_c}Q \quad (17)$$

being:

$a = k_{pE} + \omega_c + 1.5$

$b = \omega_c(k_{pE} + 1.5) + k_{iE}$

$c = k_{iE}\omega_c$

By using this model, similarly as the frequency secondary control model, the dynamic of the system can be obtained as shown in Fig. 15.

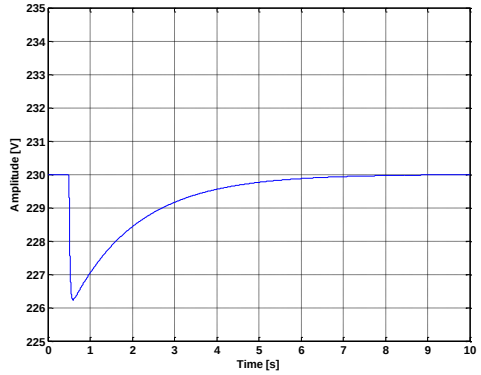

Fig. 15. Transient response of the amplitude secondary control model.

VI. Simulation Results

The proposed control was tested through proper simulations in order to validate its feasibility. The three-phase MG is shown in Fig. 11. It consists of two three-phase VSIs with all the proposed loops were simulated by using the primary and secondary control loops. The parameters are listen in Table I, the *LCL* filter parameters were chosen as:

$L_a = L_b = L_c = L = 1.8$ mH

$C_a = C_b = C_c = C = 25$ uF

$L_{oa} = L_{ob} = L_{oc} = 1.8$ mH

The nonlinear load consisted of a three-phase rectifier loaded by an LC filter (L = 84 uH and C = 235 uF) and a resistor. The MG was connected to the grid through a 5 kVA transformer with 2 mH leakage equivalent inductance.

The switching frequency of the inverters was set at 10 kHz. The control system was discretized regarding the sampling time of 10 kHz. The model has been implemented in Simulink/Matlab by using the powersys toolbox.

TABLE I
CONTROL SYSTEM PARAMETERS

Parameter	Symbol	Value	Units
Power stage			
Grid Voltage	V_g	311	V
Grid Frequency	f	50	Hz
Output Inductance	L_o	1.8	mH
Filter inductance	L	1.8	mH
Filter Capacitance	C	25	μF
Load	R_L	200/400	Ω
dc Voltage	V_{dc}	650	V
Voltage/Current P+R Control			
Voltage Loop PR	k_{pV}, $k_{rV,}$ $k_{vH5,7,11}$	0.35, 400, 4, 20, 11	
Current Loop PR	k_{pI}, $k_{rI,}$ $k_{IH5,7,11}$	0.7, 100, 30,30,30	
Primary Control			
Integral frequency droop	k_{iP}	0.0015	W/rd
Proportional frequency droop	k_{pP}	0.0003	Ws/rd
Proportional amplitude droop	k_{pQ}	0.27	VAr/V
Secondary Control			
Frequency Proportional term	k_{pF}	0.0005	Ws/rd
Frequency Integral term	k_{iF}	0.1	W/rd
Amplitude Proportional term	k_{pE}	0.0001	VAr/V
Amplitude Integral term	k_{iE}	0.11	VAr·s/V

Fig. 16 shows the voltage and current waveforms of a VSI when supplying the nonlinear load presented above. Fig. 17 exhibits the voltage harmonic content for this case. Figs. 18 and 19 show the frequency and amplitude restoration achieved by the secondary control action. Notice the both frequency and voltage rms value are slowly and successfully regulated inside the MG, hence eliminating the static deviations produced by the droop method and the virtual impedance control loops.

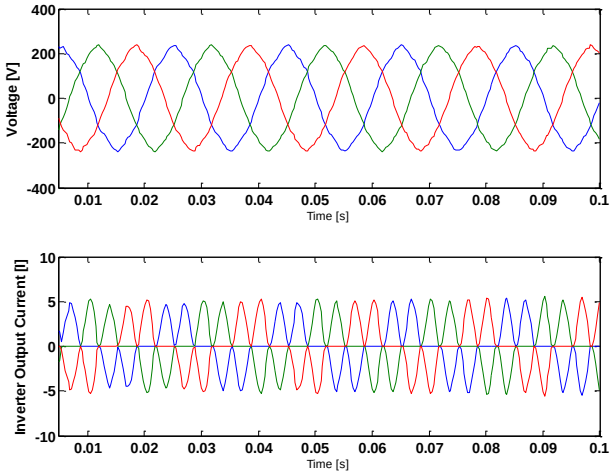

Fig. 16. Voltage (top) and current (bottom) waveforms of one VSI when supplying a nonlinear load.

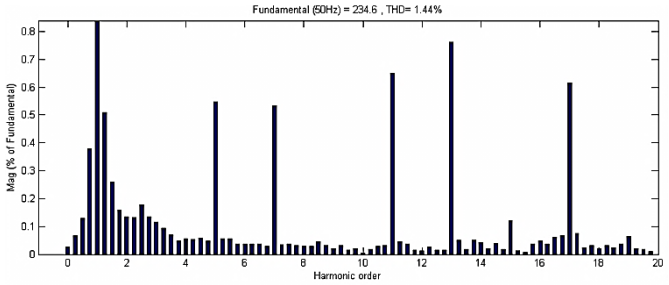

Fig. 17. Voltage harmonic content of one VSI when supplying a nonlinear load.

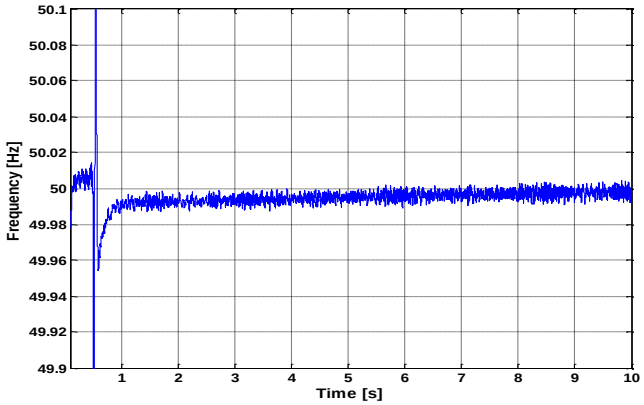

Fig. 18. Frequency restoration produced by the secondary control.

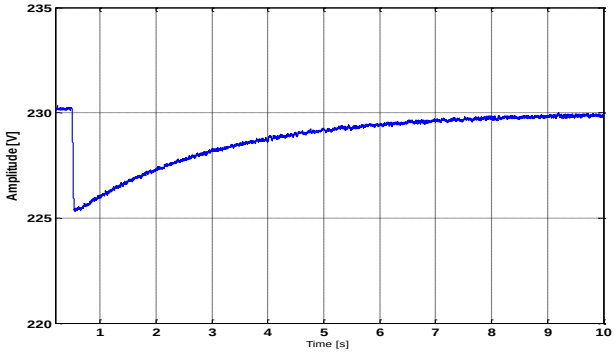

Fig. 19. Amplitude restoration produced by the secondary control.

VII. EXPERIMENTAL RESULTS

In order to test the feasibility of the theoretical studies done and the simulations obtained, an experimental MG setup was built as depict in Fig. 11 with the parameters described in Table I. Fig. 20a shows the experimental setup consisting of two Danfoss 2.2kVA inverters, voltage and current sensors, LCL filters, and a dSPACE1103 to implement the proposed control algorithms. The experimental waveforms were obtained through the dSPACE module through the Control Panel shown in Fig. 20b.

Figs. 21 and 22 show the voltage and current waveforms of a standalone VSI when supplying a nonlinear load. Fig. 23 shows the current waveforms of two parallel connected VSIs sharing the nonlinear load by using the droop method. First the two inverters are sharing the load, and suddenly the first inverter was disconnected, letting only one VSI supplying the total amount of the needed current. Figs. 24a and 24b show the frequency and amplitude deviations produced by the droop method, and the restoration of both parameters when the secondary control starts to act. Figs. 25a and 25b depict the transient response of the MG when the secondary control is continuously operating, and a load change is suddenly produced. Notice the smooth recovery toward the nominal frequency and amplitude.

Finally, Fig. 25 shows the synchronization process between the MG and the grid. It can be seen the voltage waveforms of the grid and the main grid, and the difference between them, illustrating the seamless distributed synchronization process.

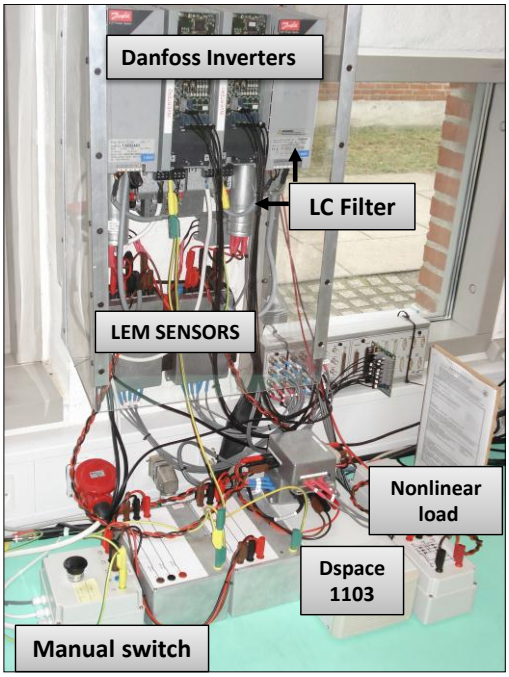

Fig. 20. Experimental setup.

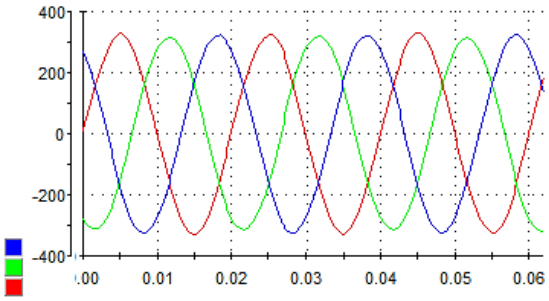

Fig. 21. Output voltage waveforms of a VSI.

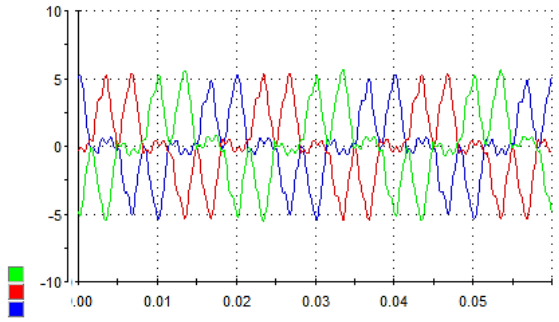

Fig. 22. Output current waveforms of a VSI.

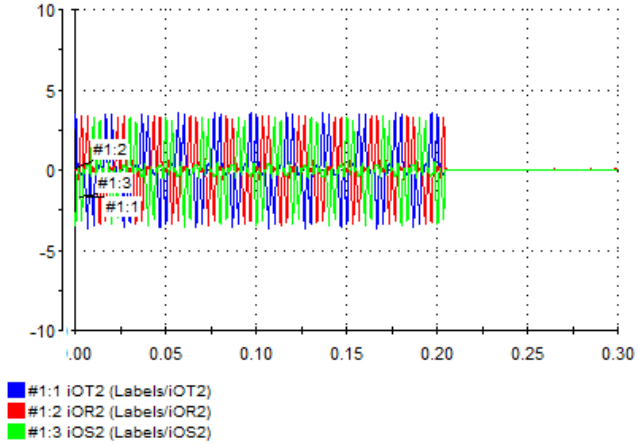

(a)

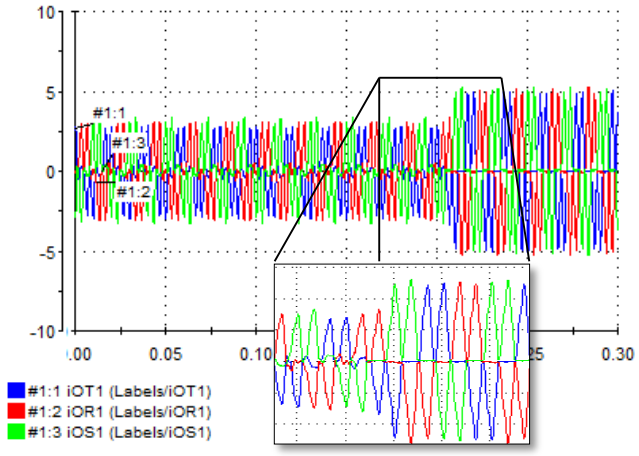

(b)

Fig. 23. Transient response of the output currents (a) inverter #1 (b) inverter #2, when inverter #1 is suddenly disconnected.

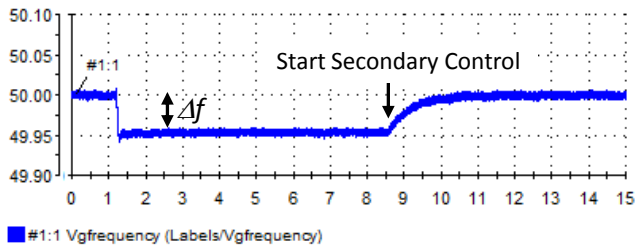

a)

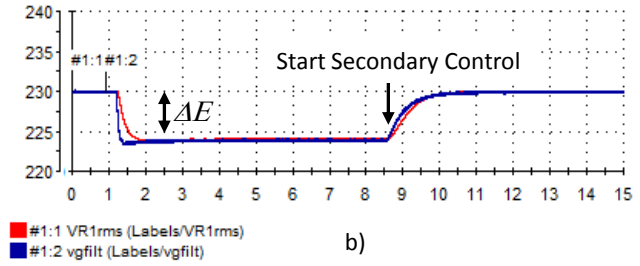

b)

Fig. 24. Frequency and amplitude deviation and restoration of the MG.

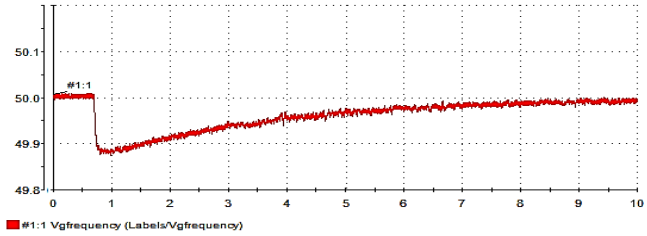

(a)

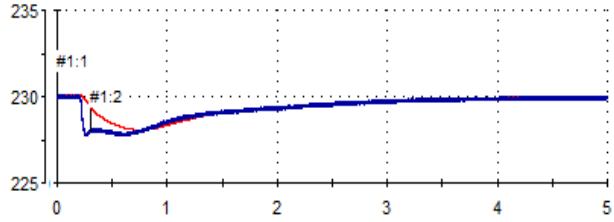

(b)

Fig. 25. Frequency and amplitude restoration of the MG.

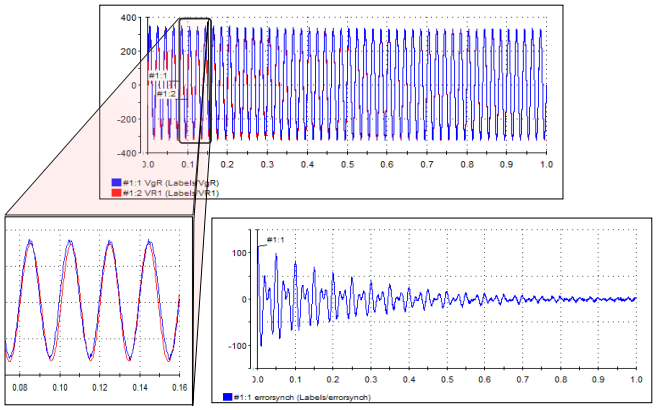

Fig. 26. Synchronization process. Top: Grid and MG Voltages, left: synchronization detail, Right: Synchronization error.

VIII. CONCLUSIONS

This paper has been proposed a hierarchical control for three-phase paralleled VSI based MGs. The control structure was based on the stationary reference frame, and organized in three main control levels. The inner control loops of the VSIs consisted of the current and voltage loops with harmonic resonant controllers. The primary control is based on the droop control and the virtual impedance concepts, which is the local controller responsible for power sharing. The secondary control is a centralized controller for the MG, which has the objective of restore frequency and amplitude deviations produced by the primary control.

The different levels of control have been modeled and the closed-loop system dynamics has been analyzed, in order to give some guidelines for the appropriate selection of the system parameters. Simulation and experimental results shown good performance of the MG control system, pointing out the hierarchical control proposed a promising approach for built next intelligent MG concepts.

REFERENCES

[1] J. C. Vasquez, J. M. Guerrero, J. Miret, M. Castilla, L. G. de Vicuña "Hierarchical Control of Intelligent Microgrids" IEEE Industrial Electronics Magazine, Dec. 2010, Volume: 4 Issue: 4, pp. 23 – 29.

[2] T.C. Green and M. Prodanovic, "Control of inverter-based micro-grids", Vol.77, no.9, 2007,pp.1204-1213.

[3] Pogaku, N.; Prodanovic, M.; Green, T.C., "Modeling, Analysis and Testing of Autonomous Operation of an Inverter-Based Microgrid," IEEE Transactions on Power Electronics, vol. 22, no. 2, 2007, pp.613-625.

[4] Teodorescu, R.; Blaabjerg, F.; Liserre, M.; Loh, P.C., "Proportional-resonant controllers and filters for grid-connected voltage source converters," IEE Proceedings on Electric Power Applications, vol.153.no.5, 2006, pp.750-762.

[5] Delghavi,M. B.; Yazdani, A.,"An Adaptive Feedforward Compensation for Stability Enhancement in Droop-Controlled Inverter-Based Microgrids," IEEE Transactions on Power Delivery, IEEE early access, April 2011.

[6] Sao, C.K.; Lehn, P.W. "Control and Power Management of Converter Fed Microgrids", IEEE Transactions on Power Systems, vol. 23, no.3, 2008, pp. 1088-1098.

[7] Barklund, E.; Pogaku, N.; Prodanovic, M.; Hernandez-Aramburo, C.; Green, T.C.; "Energy Management in Autonomous Microgrid Using Stability-Constrained Droop Control of Inverters," IEEE Transactions on Power Electronics, Vol. 23, no.5,2008, pp. 2346 – 2352.

[8] Majumder, R.; Ghosh, A.; Ledwich, G.; Zare, F., "Angle droop versus frequency droop in a voltage source converter based autonomous microgrid," Power & Energy Society General Meeting, PES '09. IEEE, 2009, pp. 1 – 8

[9] Katiraei, F. Iravani, M.R., "Power Management Strategies for a Microgrid With Multiple Distributed Generation Units," IEEE Transactions on Power Systems, vol. 21,no.4, 2006, pp. 1821

[10] J. M. Guerrero, J. C. Vasquez, J. Matas, M. Castilla, L. G. de Vicuna "Control strategy for flexible microgrid based on parallel line-inte ractive UPS systems," IEEE Transactions on Industrial Electronics, vol. 56, no. 3, March, 2009, pp. 726-736.

[11] P. L. Villeneuve, "Concerns generated by islanding," IEEE Power Energy Mag., vol. 2, no. 3, pp. 49–53, May/Jun. 2004.

[12] M. C. Chandorkar, D. M. Divan and R. Adapa, "Control of parallel connected inverters in standalone ac supply systems," IEEE Trans. on Industry Applications, vol. 29, no. 1, pp. 136-143, Jan./Feb. 1993.

[13] J. M. Guerrero, J. C. Vasquez, J. Matas, L. Garcia de Vicuna, M. Castilla "Hierarchical Control of Droop-Controlled AC and DC Microgrids – A General Approach Towards Standardization" IEEE Transactions on Industrial Electronics, vol. 51, no. 8, 2011, pp. 158 – 172.

[14] J. He and Y. Lee, "Analysis and design of interfacing inverter output virtual impedance in a low voltage microgrid," IEEE ECCE'10 Conf., Sept.2010,.pp.2857 – 2864.

[15] H. Matthias and S. Helmut, "Control of a three phase inverter feedingan unbalanced load and operating in parallel with other power sources," in Proc. EPE-PEMC'02 Conf., 2002, pp. 1–10.

[16] E. Hoff and T. Skjellnes, "Paralleled three-phase inverters," Proc. NORPIE'2004 Conf.